

A Composite Equation of State for the Modeling of Sonic Carbon Dioxide Jets in Carbon Capture and Storage Scenarios

Christopher J. Wareing, Robert M. Woolley, and Michael Fairweather

Institute of Particle Science and Engineering, School of Process, Environmental and Materials Engineering,
University of Leeds, Leeds LS2 9JT, U.K.

Samuel A. E. G. Falle

Dept. of Applied Mathematics, School of Mathematics, University of Leeds, Leeds LS2 9JT, U.K.

DOI 10.1002/aic.14102

Published online April 15, 2013 in Wiley Online Library (wileyonlinelibrary.com)

The development of a novel composite two-phase method to predict the thermodynamic physical properties of carbon dioxide (CO₂) above and below the triple point, applied herein in the context of Reynolds-Averaged Navier–Stokes computational modeling has been detailed here. A number of approaches have been combined to make accurate predictions in all three phases (solid, liquid, and gas) and at all phase changes for application in the modeling of releases of CO₂ at high pressure into the atmosphere. Predictions of a free release of CO₂ into the atmosphere from a reservoir at a pressure of 10 MPa and a temperature of 283 K, typical of transport conditions in carbon capture and storage scenarios, is examined. A comparison of the results shows that the sonic CO₂ jet that forms requires a three-phase equation of state including the latent heat of fusion to realistically simulate its characteristics. © 2013 American Institute of Chemical Engineers AIChE J, 59: 3928–3942, 2013

Keywords: complex fluids, computational fluid dynamics, green engineering, multiphase flow, nonequilibrium thermodynamics

Introduction

An essential prerequisite for computational studies of the behavior of materials is to have an accurate formulation for the description of their thermodynamic properties, applicable over a wide range of pressures and temperatures. This allows for reliable comparison of simulation to experimental data and the development of predictions for efficient and safe operations with the material in industrial applications. This particular role is typically performed by an equation of state, either optimized or specifically developed for the material in question. These equations of state are often constructed so as to give the best representation of an experimental data set. However, their accuracy is liable to be poor away from the range of the data. The effect can be pronounced and common, as users of predictive codes typically require equations of state to work as black boxes and, as long as the results are plausible, they may not concern themselves about accuracy outside the range of validity. Limitations also arise when a continuous function is unable to reproduce discontinuities at phase boundaries, for example, the change in internal energy when changing phase from liquid to solid—the latent heat of fusion. Hence, most equations of state are only valid in the gas and liquid phases above the triple point of the substance in question. For many substances, the triple point is well below the temperature range of interest, and

hence this limitation does not affect many simulations of real-world operational cases.

In the case of carbon dioxide (CO₂), however, with a triple point temperature of 216.592 K and large values of the Joule–Thomson coefficient, experiments and simulations have shown that rapid expansion from high pressures results in the expanding material dropping below this temperature. This particular “rapid expansion of supercritical solution” property has been employed in the production of micro- and nano-scale particles, as an effective cleaning process, for some time. Hence, any equation of state employed to model releases of CO₂ from high pressures to ambient atmospheric pressure must, therefore, be able to cope with material across a range of temperatures and pressures which span the critical point and the triple point. We show a schematic phase diagram for CO₂ in Figure 1.

High-pressure releases of CO₂ are of particular interest in relation to carbon capture and storage (CCS) schemes, where the intention is to capture CO₂ during production—for example, the burning of fossil fuels—and transport it to a storage site such as a subocean floor saline aquifer, thereby avoiding its release to atmosphere and any subsequent green house gas effects. The transport process is most efficient in the liquid phase, typically at pressures of 10 MPa or more to avoid problems of approaching the phase boundary during normal operations. However, the dispersion characteristic of a leak of such high-pressure material is an issue, as in the atmosphere, CO₂ has a toxic effect above 5% concentration and causes hyperventilation above 2%.^{2,3}

The Peng–Robinson equation of state⁴ and related equations extend the ideal equation of state in a simple cubic form, with

Correspondence concerning this article should be addressed to C. J. Wareing at C.J.Wareing@leeds.ac.uk.

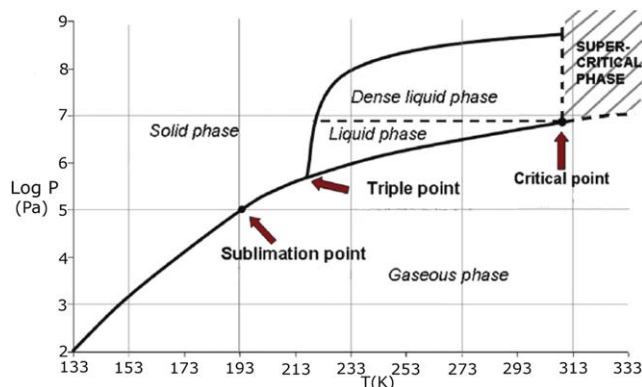


Figure 1. Schematic of the phase diagram for CO₂¹.

[Color figure can be viewed in the online issue, which is available at wileyonlinelibrary.com.]

parameters expressed in terms of the critical properties and the acentric factor. The chief aim is to provide reasonable accuracy in the gas and liquid phases, particularly near the critical point. The Span and Wagner equation of state for CO₂⁵ is a complex equation (~50 terms) explicit in the Helmholtz free energy. It consists of a simultaneous nonlinear fit to all of the available data on the thermodynamic properties of CO₂. In the temperature range from the triple point up to 523 K and 30 MPa, the estimated uncertainty of the equation ranges from ±0.03 to ±0.05% in the density, ±0.03 to ±1% in the speed of sound, and ±0.15 to ±1.5% in the isobaric heat capacity. It is considered the most accurate equation of state available for CO₂ at the present time and is the basis of the commercial GERG⁶ and industry standard REFPROP software packages. For the gas and liquid phases, it is the benchmark to measure against.

The Peng–Robinson equation of state is satisfactory for the gas phase, but when compared to Span and Wagner, it is not so for the condensed phase, as we will demonstrate in the next section. Furthermore, it is not accurate for the gas pressure below the triple point and, in common with any single equation, it does not account for the discontinuity in properties at the triple point. In particular, there is no latent heat of fusion. Span and Wagner give a formula for the Helmholtz free energy that is valid for both the gas and liquid phases above the triple point, but it does not take account of experimental data below the triple point, nor does it give the properties of the solid. In any case, the formula is too complicated to be used efficiently in any computational fluid dynamics (CFD) code.

There is a clear need for a computationally efficient equation of state that can accurately span the critical point and the triple point, with continuous derivatives throughout the range, for use in CCS scenarios. It is the first objective of this article to introduce a computationally efficient composite method for the accurate modeling of releases of CO₂ as a two-phase fluid, modeling the vapor phase and the condensed phase, including the latent heat of fusion to model both the liquid and solid phases. It is the second objective to demonstrate the improved performance of this composite approach over other common computationally simple approaches applied to the near-field of a high-pressure release of CO₂, of relevance to the CCS industry. Specifically, we consider also the ideal equation of state and the Peng–Robinson equation of state. The focus of the Results section is on the comparison of these two equations of state to the new composite approach. Accuracy of the equation of

state is not only important for fundamental physical investigations, but also for safety assessment of CO₂ pipelines where accurate knowledge of the near-field structure of an escaping CO₂ jet may be necessary for producing reliable predictions of subsequent dispersion behavior, necessary for industrial safety modeling and risk assessment.

The layout of this article is as follows. The section Inviscid Flow Model describes the format of an equation of state and the Peng–Robinson equation of state for CO₂, highlighting its limitations and introduces the improved composite equation of state formulation for three phases. The Computational Model describes the computational method which we have developed to simulate atmospheric releases of CO₂ and its implementation into an appropriate Reynolds-Averaged Navier–Stokes (RANS) equation solver (the MG code). The Testing and Validation section sets out our testing and validation of this composite equation of state. The Results section presents the results of modeling a high-pressure release into ambient air, demonstrating the improved performance of the composite method over ideal gas and two-phase (Peng–Robinson) equation of state approaches. The Discussion section discusses these results and our conclusions are drawn in the Conclusions section.

Inviscid Flow Model

The RANS equations for an inviscid flow model are

$$\frac{\partial \rho}{\partial t} + \nabla \cdot (\rho u) = 0 \quad \text{equation of continuity} \quad (1)$$

$$\frac{\partial \rho C}{\partial t} + \nabla \cdot (\rho C u) = 0 \quad \text{scalar transport} \quad (2)$$

$$\frac{\partial \rho u}{\partial t} + \rho(u \cdot \nabla)u + \nabla p = 0 \quad \text{momentum} \quad (3)$$

$$\frac{\partial e}{\partial t} + \nabla \cdot [u(e+p)] = 0 \quad \text{energy} \quad (4)$$

where e is the total energy per unit volume. We employ these equations in this work.

Equations of State

We assume an equation of state of the form

$$p = p(v, T) \quad (5)$$

where p is the pressure, v is the molar volume, and T is the temperature.

Following previous authors (e.g., Span and Wagner), we choose to work with the Helmholtz free energy, F , in terms of T and v as all other thermodynamic properties can readily be obtained from F . The Helmholtz free energy per mole for an ideal gas is given by

$$F = F_i = -RT \left[\frac{1}{(\gamma-1)} \ln \left(\frac{T}{T_0} \right) + \ln \left(\frac{v}{v_0} \right) \right] \quad (6)$$

where T_0 and v_0 are for some reference state for which the ideal equation of state is valid.

We can now use the standard relation

$$p = - \left(\frac{\partial F}{\partial v} \right)_T \quad (7)$$

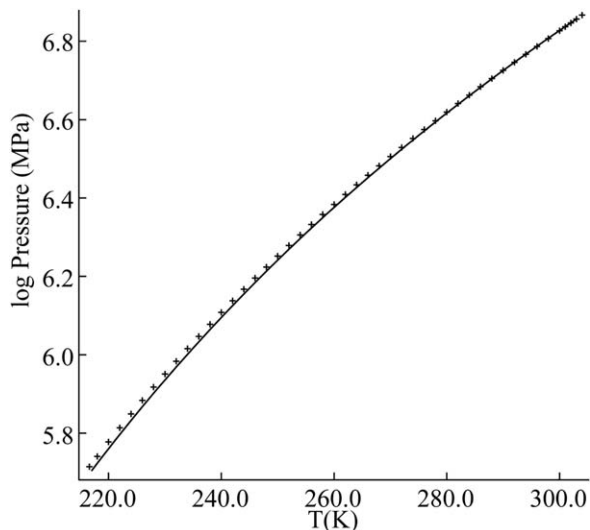


Figure 2. Predictions of saturation pressure obtained using the Peng–Robinson (line) and the Span and Wagner (markers) equations of state.

to obtain F for any other equation of state from

$$F(T, v) = F_i(T, v_0) - \int_{v_0}^v p \, dv \quad (8)$$

This assumes that $F(T, v_0) = F_i(T, v_0)$, which is valid provided v_0 is sufficiently large.

As the entropy is given by

$$S = - \left(\frac{\partial F}{\partial T} \right)_v \quad (9)$$

the internal energy is hence given by

$$U(T, v) = F + TS = F - T \left(\frac{\partial F}{\partial T} \right)_v \quad (10)$$

The adiabatic sound speed of a pure component is given by

$$c = \left[\left(\frac{\partial p}{\partial \rho} \right)_s \right]^{1/2} = \left[-v^2 \left(\frac{\partial p}{\partial v} \right)_s \right]^{1/2} \quad (11)$$

and it can be shown that

$$\left(\frac{\partial p}{\partial v} \right)_s = \left(\frac{\partial p}{\partial v} \right)_T - \left(\frac{\partial p}{\partial T} \right)_v \left(\frac{\partial S}{\partial v} \right)_T \left(\frac{\partial T}{\partial S} \right)_v$$

In equilibrium on the saturation curve, $p(T)$ satisfies the Clapeyron equation

$$\left(\frac{\partial p}{\partial T} \right)_{\text{sat}} = \left[\frac{S(T, v_c) - S(T, v_v)}{v_c - v_v} \right] \quad (12)$$

where $v_c(T)$ and $v_v(T)$ are the molar volumes of the liquid/solid and gas, respectively.

Ideal gas equation of state

The ideal gas equation of state can be expressed as

$$p = p(v, T) = \frac{RT}{v} \quad (13)$$

Peng–Robinson equation of state

The Peng–Robinson equation of state⁴ extends the ideal equation and is

$$p = p(v, T) = \frac{RT}{(v-b)} - \frac{a\delta}{(v^2 + 2bv - b^2)} \quad (14)$$

where a , b , and δ are given by

$$a = 0.45724 \frac{(RT_{\text{crit}})^2}{p_{\text{crit}}}$$

$$b = 0.07780 \frac{RT_{\text{crit}}}{p_{\text{crit}}}$$

$$\delta = \left[1 + (0.37464 + 1.54226\omega - 0.26992\omega^2) \left(1 - \sqrt{\frac{T}{T_{\text{crit}}}} \right) \right]^2 \quad (15)$$

Here p_{crit} is the critical pressure, T_{crit} is the critical temperature, and ω is the acentric factor. For CO_2 , these are $p_{\text{crit}} = 7.3773 \text{ MPa}$, $T_{\text{crit}} = 304.1282 \text{ K}$, and $\omega = 0.228$.

Figure 2 shows the saturation pressure predicted by the Peng–Robinson and Span and Wagner⁵ equations of state. From Figure 2, it can be seen that the Peng–Robinson and Span and Wagner equations agree rather well, but, as can be seen from Figure 3, the liquid density given by these two equations does not agree nearly so well. On the other hand, Figure 3 also shows that the gas densities are in close accord.

Improved composite equation of state

We have constructed a composite equation of state in which the gas phase is computed from the Peng–Robinson equation of state. The liquid phase and saturation pressure are calculated from tabulated data generated with the Span and Wagner equation of state and the best available source of thermodynamic data for CO_2 , the Design Institute for Physical Properties (DIPPR®) 801 database (<http://www.aiche.org/dippr>), academic access to which can be gained through the Knovel library (<http://why.knovel.com>).

The properties of gaseous CO_2 are obtained from the Peng–Robinson equation of state with the parameters given

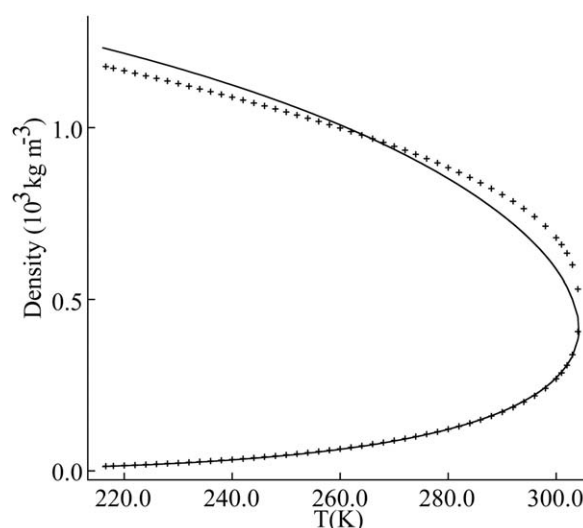


Figure 3. Predictions of density on the saturation curve obtained using the Peng–Robinson (line) and the Span and Wagner (markers) equations of state.

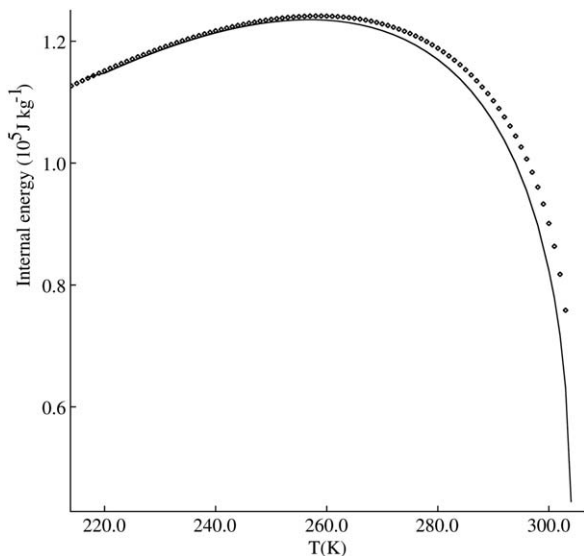


Figure 4. Predictions of internal energy of CO₂ gas on the saturation line.

Line: adjusted Span and Wagner equation of state; **markers:** Peng–Robinson equation of state.

in the previous section. The internal energy in the gas phase is computed using the following expression for the specific heat at constant volume

$$C_v = A + BT + CT^2 \quad (\text{Jkg}^{-1}\text{K}^{-1}) \quad (16)$$

where here $A=469.216$, $B=0.6848$, and $C=1.211 \times 10^{-4}$. This expression has been obtained by fitting to the internal energy data in the DIPPR® Project 801 database over the temperature range $150 \leq T \leq 300\text{K}$. The internal energy of the gas at the reference state used by Span and Wagner is then $U_0=1.71403 \times 10^5 \text{Jkg}^{-1}$ at $T=298.15\text{K}$, and $p=1.01325 \times 10^5 \text{Pa}$.

The internal energy of the liquid is taken from Span and Wagner, except that we add $1.4422 \times 10^4 \text{Jkg}^{-1}$ to the Span and Wagner values to ensure that differences between the gas and liquid internal energies on the saturation line in our model are close to theirs. Figure 4 shows that the agreement is very good in the crucial temperature range from the triple point to 280 K. The pressure dependence of the internal energy of the liquid is modelled via a quadratic fit to the tabulated data presented in Span and Wagner.

The sound speed for the liquid is taken from Span and Wagner and is assumed to be equal to that on the saturation line. The pressure dependence of the density of the liquid is calculated from the density and sound speed on the saturation line in combination with a quadratic fit to the tabulated data presented in Span and Wagner.

For the internal energy of the solid, we use

$$U = -4.04533 \times 10^5 - 36.4215(T - T_{\text{trip}}) + 12.3027(T^2 - T_{\text{trip}}^2)/2 + 0.02882(T^3 - T_{\text{trip}}^3)/3 \quad (\text{Jkg}^{-1}) \quad (17)$$

This has been obtained from the DIPPR® 801 Database tables along with the latent heat of fusion at the triple point of $204.932 \text{kJ kg}^{-1}$. Note that we have ignored the pressure dependence and the difference between the internal energy and the enthalpy for the solid as these are negligible.

To calculate the solid density, we use the same approach as Witlox et al.⁷

$$\rho = 1289.45 + 1.8325T \quad (\text{kg m}^{-3}) \quad (18)$$

again based on property information from the DIPPR® 801 Database. From Liu,⁸ the solid sound speed at atmospheric pressure and 296.35 K is 1600m s^{-1} and we assume that this is independent of temperature and pressure. Note that the results are extremely insensitive to the solid density and sound speed.

The saturation pressure above the triple point is taken from Span and Wagner. Below the triple point, they give the following empirical formula

$$p_s(T) = p_{\text{trip}} \exp \left\{ \left[a_1 (1.0 - T/T_{\text{trip}}) + a_2 (1.0 - T/T_{\text{trip}})^{1.9} + a_3 (1.0 - T/T_{\text{trip}})^{2.9} \right] \frac{T_{\text{trip}}}{T} \right\} \quad (\text{Pa}) \quad (19)$$

where $T_{\text{trip}}=216.592\text{K}$ is the temperature of the triple point, $p_{\text{trip}}=0.518 \times 10^6 \text{Pa}$ is the pressure at the triple point, and $a_1=-14.740846$, $a_2=2.4327015$, and $a_3=-5.3061778$.

Figure 5 shows the internal energy of the gas and condensed phases on the saturation line. The transition from liquid to solid has been smoothed over 4 K with a hyperbolic tangent function centered on the triple point. This has been done for computational reasons to ensure the function and its differentials are smooth.

The Computational Model

Homogeneous mixtures

As any computational model of CO₂ releases has to deal with mixtures of air and CO₂ in liquid/solid and gas form, we need to derive the appropriate equations for such mixtures. Let α be the mass fraction of the CO₂ that is in liquid/solid form and β the total mass fraction of CO₂. The mass fraction of air is then $1 - \beta$. We assume that the mixture is

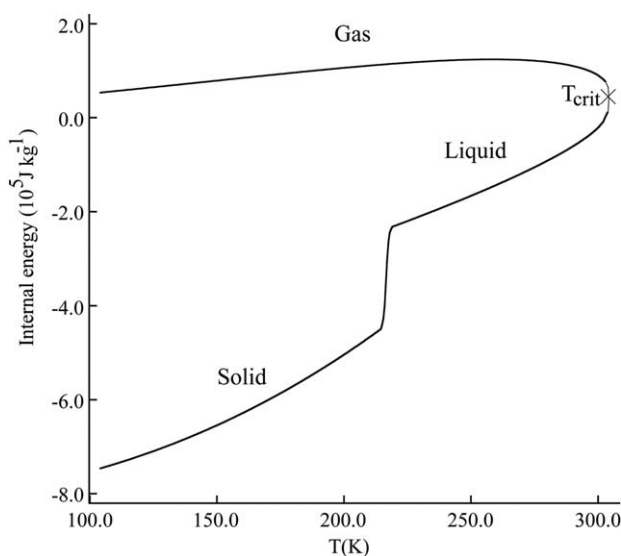


Figure 5. Predictions of internal energy on the saturation line for the composite equation of state.

T_{crit} marks the critical temperature. The triple point temperature can be identified by the steep connection between the liquid and solid phases—the latent heat of fusion.

homogeneous, that is, that the solid/liquid and gas phases are well mixed and that the liquid drops or solid particles are sufficiently small. We also assume for the purposes of elucidating the differences between equations of state that the air is dry and contains no water vapor.

With these assumptions, in unit volume the mass of liquid-/solid-phase CO₂ is

$$m_c = \alpha\beta\rho$$

which means that the volume of liquid/solid CO₂ is

$$v_c = \frac{\alpha\beta\rho}{\rho_c}$$

where ρ_c is the density of the liquid/solid condensed form of CO₂. The volume of gaseous CO₂ and air is then

$$v_g = 1 - v_c = 1 - \frac{\alpha\beta\rho}{\rho_c}$$

As the masses of gaseous CO₂ and air per unit volume are

$$m_v = \beta(1-\alpha)\rho, \quad m_a = (1-\beta)\rho$$

their densities are

$$\rho_a = \frac{m_a}{v_g} = \frac{(1-\beta)\rho}{[1-\alpha\beta\rho/\rho_c]} \quad (20)$$

$$\rho_v = \frac{m_v}{v_g} = \frac{\beta(1-\alpha)\rho}{[1-\alpha\beta\rho/\rho_c]} \quad (21)$$

The total gas density is then

$$\rho_g = \rho_a + \rho_v = \frac{(1-\alpha\beta)}{[1-\alpha\beta\rho/\rho_c]}\rho \quad (22)$$

and one can show that

$$\frac{1}{\rho} = \frac{\alpha\beta}{\rho_c} + \frac{(1-\alpha\beta)}{\rho_g} \quad (23)$$

Mixture frozen sound speed

If any thermodynamic change is so rapid that the liquid and gas mass fractions remain constant, then the relevant sound speed is the frozen sound speed.

Differentiating Eq. 23 with respect to p at constant entropy gives

$$\frac{1}{\rho^2 c^2} = \frac{\alpha\beta}{\rho_c^2 c_c^2} + \frac{(1-\alpha\beta)}{\rho_g^2 c_g^2} \quad (24)$$

where c_c and c_g are the adiabatic sound speeds for the liquid/solid and gas phases, respectively. c_c is given by Eq. 11 with the liquid/solid equation of state.

For the gas we have

$$dp = c_a^2 d\rho_a + c_v^2 d\rho_v \quad (25)$$

where c_a and c_v are the sound speeds of air and gaseous CO₂. Differentiating Eqs. 20 and 21 with respect to ρ gives

$$d\rho_a = \frac{(1-\beta)}{(1-\alpha\beta\rho/\rho_c)^2} d\rho, \quad d\rho_v = \frac{\beta(1-\alpha)}{(1-\alpha\beta\rho/\rho_c)^2} d\rho$$

Using these to eliminate ρ_a and ρ_v in Eq. 25 gives

$$\frac{dp}{d\rho} = c_g^2 = \frac{1}{(1-\alpha\beta\rho/\rho_c)^2} [c_a^2(1-\beta) + c_v^2\beta(1-\alpha)] \quad (26)$$

This sound speed plays a role if it takes a finite time for the liquid and gas to come into equilibrium.

Equilibrium sound speed

It is also necessary to calculate the adiabatic sound speed for a pure CO₂ liquid/solid-gas mixture when it remains in equilibrium. We start from

$$v = \alpha v_c + (1-\alpha)v_g$$

Differentiating this gives

$$dv = (v_c - v_g)d\alpha + \alpha dv_c + (1-\alpha)dv_g \quad (27)$$

$d\alpha$ can be determined from the fact that this is an isentropic process. We have

$$S = \alpha S_c + (1-\alpha)S_g$$

Differentiating this gives

$$dS = (S_c - S_g)d\alpha + \alpha dS_c + (1-\alpha)dS_g = 0 \quad (28)$$

which implies

$$d\alpha = \frac{1}{(S_g - S_c)} [\alpha dS_c + (1-\alpha)dS_g] \quad (29)$$

The differentials of the entropy are given by

$$dS_{c,g} = \left(\frac{\partial S_{c,g}}{\partial T}\right)_v dT + \left(\frac{\partial S_{c,g}}{\partial v}\right)_T dv_{c,g} \quad (30)$$

To get differentials of the volumes, we start from

$$dp = \left(\frac{\partial p}{\partial T}\right)_{\text{sat}} dT = \left(\frac{\partial p}{\partial T}\right)_v dT + \left(\frac{\partial p}{\partial v}\right)_T dv_{c,g} \quad (31)$$

which then gives

$$dv_{c,g} = \left[\left(\frac{\partial p}{\partial T}\right)_{\text{sat}} - \left(\frac{\partial p}{\partial T}\right)_v \right] \frac{dT}{(\partial p/\partial v)_T} \quad (32)$$

Using 29, 30 and 32 in 27 gives dv in terms of dT . As we know dp in terms of dT from 31, this gives $(\partial p/\partial v)_S$ and hence the sound speed.

Homogeneous equilibrium model

In such a model, all phases are assumed to be in dynamic and thermodynamic equilibrium, that is, they all move at the same velocity and have the same temperature. In addition, the pressure of the CO₂ gas is assumed to be equal to the saturation pressure whenever the condensed phase is present. The pressure of the condensed phase CO₂ is assumed to be equal to the combined pressure of gaseous CO₂ and air (the total pressure). These assumptions are reasonable provided the CO₂ liquid drops or solid particles are sufficiently small. It should be noted that for small droplets, the Kelvin effect will cause the vapor pressure to deviate from the saturated pressure. However, calculation of the Kelvin effect relies on accurate knowledge of the surface energy of CO₂ droplets—currently unknown, see for example.⁹ In line with this previous work, we assume this is zero and ignore the Kelvin effect. Future work will consider this in more detail, but for

now we consider both an equilibrium model and a homogeneous relaxation model in the next section.

As the code into which this model will be introduced is conservative, it works with the total energy per unit volume

$$e = \rho U + \frac{1}{2} \rho u^2 \quad (33)$$

where ρ is the total density, U is the internal energy per unit mass and u is the magnitude of velocity. The code also computes the total mass fraction of CO_2 , β .

To integrate the conservation equations, it is necessary to compute the mixture pressure (p), temperature (T), mass fraction of liquid/solid CO_2 (α), density of CO_2 gas (ρ_v), density of air (ρ_a), and density of liquid/solid CO_2 (ρ_c) from ρ , U and β . The densities of air and CO_2 gas are given by Eqs. 20 and 21.

As the gaseous CO_2 is in equilibrium with liquid/solid CO_2 , we have

$$p_s(T) = p(\rho_v, T) \quad (34)$$

where $p_s(T)$ is the saturation pressure and $p(\rho_v, T)$ is the pressure given by the equation of state.

The mixture pressure is given by

$$p_{\text{mix}} = \frac{\rho_a RT}{w_a} + p_s(T) \quad (35)$$

The total internal energy per unit mass is given by

$$U = \frac{(1-\beta)RT}{w_a(\gamma_a-1)} + (1-\alpha)\beta U(\rho_v, T) + \alpha\beta U(\rho_c, T) \quad (36)$$

where w_a and γ_a are the molecular weight and ratio of specific heats for air. Note that we have used the ideal equation of state for air.

In general, mixing occurs at pressures close to atmospheric, so one can use the ideal equation of state for the gaseous CO_2

$$p(\rho_v, T) = \frac{\rho_v RT}{w_c} \quad (37)$$

and

$$U(\rho_v, T) = \frac{RT}{w_c(\gamma_c-1)} \quad (38)$$

where w_c and γ_c are the molecular weight and ratio of specific heats for CO_2 .

The density of the liquid/solid can be obtained from

$$\rho_c = \rho_c(p_{\text{mix}}, T) \quad (39)$$

which is obtained from the equation of state.

Equations 20–36, and 39 are solved for T , p_{mix} and α using a 2D Newton–Raphson iteration.

This procedure is somewhat simpler for pure CO_2 ($\beta=1$) on the saturation line. We then have

$$\frac{1}{\rho} = \frac{\alpha}{\rho_c} + \frac{(1-\alpha)}{\rho_v} \quad (40)$$

and

$$U = \alpha U(\rho_c, T) + (1-\alpha)U(\rho_v, T) \quad (41)$$

Equations 40 and 41 give T and α as $\rho_c = \rho_c(T)$ and $\rho_v = \rho_v(T)$ on the saturation curve.

Homogeneous relaxation model

The vapor will only be in equilibrium if the size of the liquid drops or solid particles is sufficiently small. There are some indications that this will not be true, in particular for test calculations in which the rupture size is of the order of centimeters. A full model will require the inclusion of drops or particles and is beyond the scope of this article. For the current model, it is possible to derive a simple submodel for the relaxation to equilibrium by assuming that the condensed phase mass fraction is given by

$$\frac{\partial \rho \alpha}{\partial t} + \nabla \cdot (\rho \alpha u) - \nabla \cdot (\mu_T \nabla \alpha) = S_\alpha \quad (42)$$

and ignoring temperature relaxation. The source term is then

$$S_\alpha = \beta \frac{(p_v - p_s)}{\tau p_s} \quad (43)$$

where p_v is the vapor pressure, p_s is the saturation pressure and τ is a relaxation time. This is consistent with the form of evaporation/condensation rate given by Jacobson.¹⁰ In the simulations presented here, we employ a relaxation time of $\tau = 10^{-3}$, ensuring a rapid relaxation to equilibrium, appropriate in the initial expansion. Future work will consider the implications of increasing this timescale beyond the Mach shock and more accurately modeling the post Mach shock flow.

In this case, obtaining the temperature from the conserved variables is somewhat simpler than for the homogeneous model as α is already known. We can assume that the solution is insensitive to ρ_c and then use a 2D Newton–Raphson method to solve Eqs. 20, 21, and 36 for T and p_{mix} . ρ_c can be updated within each iteration from Eq. 39.

Numerical solution method

All three equations of state were implemented into the Adaptive Mesh Refinement (AMR) RANS hydrodynamic-code MG, developed by Falle.¹¹ The code employs an upwind, conservative shock-capturing scheme and is able to employ multiple processors through parallelization with the Message Passing Interface (MPI) library. Integration in time proceeds according to a second-order accurate Godunov method.¹² In this case, a Harten Lax van–Leer^{13,14} (HLL) Riemann solver has been employed to aid the implementation of complex equations of state. The disadvantage of the HLL solver is that it is more diffusive for contact discontinuities; this is not important here as the contact discontinuities are in any case diffused by the artificial viscosity. The artificial viscosity is required to ensure shocks travel at the correct speed in all directions and is at a very low level, decreasing with increasing resolution. The AMR method¹⁵ employs an unstructured grid approach, requiring an order of magnitude less memory and giving an order of magnitude faster computation times than structured grid AMR. The two coarsest levels—0 and 1—cover the whole computational domain, finer grids need not do so. Refinement or derefinement depends on a given tolerance. Defragmentation of the AMR grid in hardware memory is performed at every time-step, gaining further speed improvements for negligible cost through reallocation of cells into consecutive memory locations. Figure 6 demonstrates this technique, and where there are steep gradients of variable magnitudes such as at flow boundaries or discontinuities such as the Mach disc, (demonstrated by the

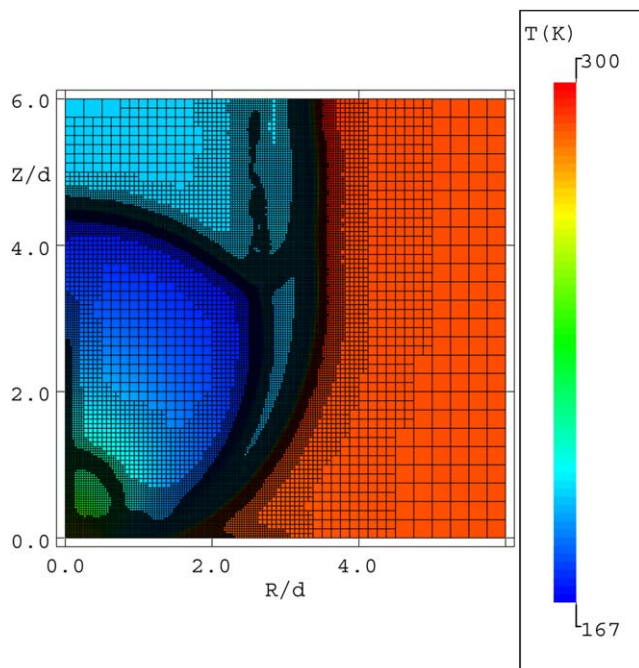


Figure 6. AMR grid when simulating a CO₂ release.

This figure shows levels 1–5 of the AMR, level 0 cells (0.5D on a side) are only employed outside the pictured domain. [Color figure can be viewed in the online issue, which is available at wileyonlinelibrary.com.]

plot of temperature in Figure 6) the mesh is more refined than in areas of the free stream in the surrounding fluid. Each layer is generated from its predecessor by doubling the number of computational cells in each spatial direction. This technique enables the generation of fine grids in regions of high spatial and temporal variation, and conversely, relatively coarse grids where the flow field is numerically smooth. Figure 6 shows the population of five levels of AMR when simulating a CO₂ release at sonic velocity.

Testing and Validation

To elucidate the physical differences in realistic situations between the new composite equation of state, the Peng–Robinson equation of state and an ideal equation of state, an identical scenario with identical initial conditions must be simulated with each. A comparison of the results will reveal the performance of each approach. Ideally, further comparisons should be performed against experimental results. However, experimental measurements of high-pressure releases of CO₂ are scarce and we have been unable to find any published in a form which would allow for direct comparison of the near-field structure of a release.

Initial conditions

We wish to elucidate the physics associated with releases of CO₂ for conditions typical of those under consideration in relation to CCS schemes. Transportation within CCS scenarios is likely to be undertaken along high-pressure pipelines, similar to those used in the natural gas industry, with typical operating conditions in either liquid or supercritical phase, at operating pressures around 10–15 MPa.¹⁶

We have calculated thermodynamic pipeline decompressions from three representative pipeline conditions, specified in Table 1 using a method similar to that presented in Ref. 17.

Table 1. Representative Pipeline Conditions for CO₂ in the Gas, Liquid, and Supercritical Phases

Phase	Pressure (MPa)	Temperature (K)
Liquid	7.0	283.15
Supercritical	10.0	313.15
Gas	3.0	283.15

Figure 7 shows the thermodynamic decomposition paths from these three initial conditions in a pressure–temperature p – T diagram. All three conditions follow isentropic adiabats in the p – T diagram which intersect the saturation curve at different locations and, as this is a homogeneous equilibrium model, the thermodynamic conditions at the exit plane then adhere to the saturation curve during the steady-state stage of the release and also consequently as the temperature reduces. The supercritical release intersects the saturation curve at only a slightly lower temperature and pressure than the critical point. We have chosen a single set of initial exit plane conditions on the saturation line that are representative of these high-pressure releases. These initial conditions are specified in Table 2, and

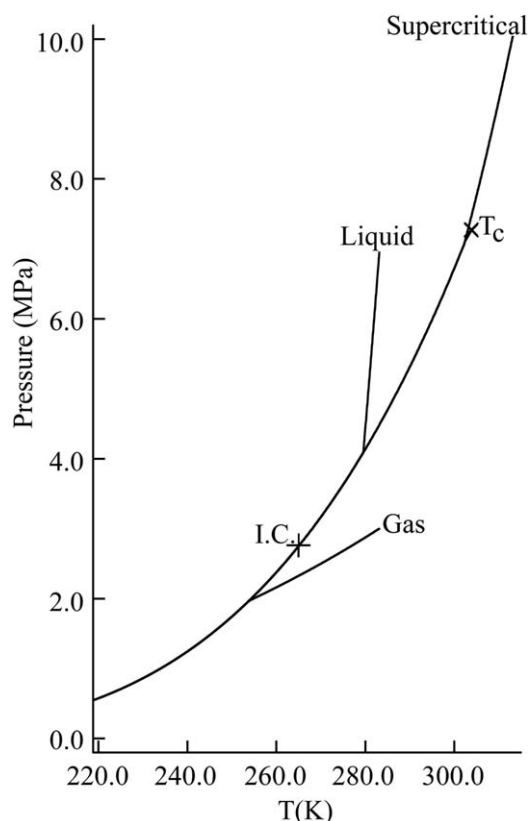


Figure 7. Predicted thermodynamic decomposition paths on a pressure–temperature diagram for the three representative pipeline conditions.

The start of the line at each condition titles indicates the start of the decomposition path for each case. The critical point is also marked (T_c)—note that the decomposition path from the supercritical state hits the saturation line just below the critical point. The saturation line (phase transition line) is indicated by the curve starting at T_c . I.C. marks the initial conditions used in this work that are representative of decompressions from reservoirs or pipelines containing high-pressure liquid or supercritical CO₂.

Table 2. Initial Conditions—Representative of Releases from Reservoirs or Pipelines Containing High Pressure Liquid or Supercritical CO₂

Initial Conditions	
Reservoir pressure	10.00 MPa
Reservoir temperature	283.15 K
Reservoir CO ₂ fraction	100.00%
Condensed phase fraction	100.00%
Exit plane pressure	2.79 MPa
Exit plane temperature	265.51 K
Exit plane velocity	71.62 m s ⁻¹
Exit plane Mach number	1.18
Exit plane CO ₂ fraction	100.00%
Exit plane condensed phase fraction	82.43%

are typical of those conditions that would occur in the exit plane of an accidental puncture in a high-pressure pipeline.^{18,19} To compare performance between the three equations of state, pressure and mass-flow must be conserved at the orifice. Hence, the temperature and velocity conditions are the same for the Peng–Robinson and composite equations of state, but considerably different when conserving pressure and mass-flow with the ideal equation. The ideal equation of state has been included as it is employed in a variety of engineering applications for modeling gas dispersion.

In computationally simulating this release, we have employed a two-dimensional (2-D) cylindrical polar axisymmetric coordinate system with a domain extending to 20 exit diameters in both the r and z directions. The coarsest grid level contains 40×40 cells. Six levels of AMR have been employed to fully resolve the near-field structure, giving 32 cells across the release diameter. The initial state of the fluid in the domain consists entirely of stationary air at a pressure of 10⁵ Pa and a temperature of 290 K. Conditions in air are calculated via an ideal gas equation of state with $\gamma_a=7/5$. We use $\gamma_c=1.28$ for CO₂. Boundary conditions have been specified as symmetric at $r=0$, free-flow at $r=20$ and $z=20$, and fixed at $z=0$. Given that vortex structures may be present in the jet as it reaches steady state, velocities that lead to inflow can occur at the free-flow boundary at $z=20$. Hence, the boundary condition is adjusted to ensure that only ambient air can flow into the domain, with the same properties as the initial condition, and no CO₂. The exit conditions in Table 2 are enforced on every time step at the $z=0$ boundary for $r < 0.5$.

The simulations performed employed an artificial viscosity dependent on grid resolution to avoid numerical instabilities. This viscosity decreases with the maximum number of AMR levels used. The simulations presented below used six levels of AMR and hence a very low level of artificial viscosity. Steady state was achieved through starting simulations at the coarsest level and establishing a steady state before adding another grid level and again advancing in time with the same constant exit conditions until steady state was again achieved. The simulations shown below are convergent and show little variation with exit pressure, temperature, and velocity.

Results

In this section, we compare the results of simulating the near-field structure from a high-pressure CO₂ release with the ideal, Peng–Robinson and composite equations of state. We show 2-D r - z plots of the near-field from the simulations

on a subset of the computational domain from 0 to 6 release orifice diameters in both r and z . This subset reveals the structure of the near-field, defined here as the region including the rapid expansion and Mach shock. A short post-shock region that is representative of the conditions in the rest of the downstream jet is also included. Other representations of the data include one-dimensional (1-D) cuts along the axis of the jet ($r=0$) to show changing conditions through the Mach shock.

Figure 8 shows the near-field temperature structure resulting from the three different equations of state approaches. Note that the initial temperature of the ideal model is different because pressure and mass-flow have been conserved in the initial condition. The ideal equation of state predicts a width of the jet at the Mach shock 15% narrower than the Peng–Robinson equation of state, and 23% narrower than the composite equation of state. The three equations of state also clearly lead to qualitatively different temperature distributions. In the lower right panel of this figure, we compare the temperatures along the jet axis. The ideal approach (dotted line) predicts a lower temperature—down to 55 K just before the Mach shock—in the expansion region, as compared to the Peng–Robinson (dashed line) and composite (solid line) equations of state, which predict 155 and 168 K, respectively. Postshock, when the pressure in the jet is close to atmospheric, solid and gaseous CO₂ coexist. In a homogeneous equilibrium model, such as the one presented here into which all three equations of state approaches were implemented, a mixture of pure two-phase CO₂ at atmospheric pressure must be on the saturation curve, at what is defined as the sublimation temperature: 194.675 K for CO₂.²⁰ All three models predict 100% CO₂ at approximately atmospheric pressure in the core of the jet immediately after the Mach shock, thus allowing for an excellent test—the core of the jet should be at the sublimation temperature. The ideal equation of state predicts a high core temperature around 247.5 K, whereas the Peng–Robinson and composite equations of state predict 185.3 and 193.9 K, respectively. The composite model is, therefore, in excellent agreement with the sublimation temperature, the slight difference due to the fact that the pressure immediately after the Mach shock is approximately 5% lower than atmospheric. The low temperature in the Peng–Robinson equation case is a demonstration of how the model-predicted saturation pressure diverges from the real saturation pressure going below the triple point.

The ideal equation of state also predicts a warm core and a cold annulus around the jet, unlike the Peng–Robinson and composite equations of state where the temperature is approximately constant across the entire width of the jet. The three different equations of state also predict different locations of the Mach shock. The Peng–Robinson and composite equations of state are in reasonable agreement in terms of downstream distance, whereas the ideal equation of state would appear to be in disagreement with both. These differences in structure highlight how unsuitable an ideal gas approach is for modeling the near-field jet structure of high-pressure CO₂ releases. The Peng–Robinson equation of state employs an accurate model in the gas and liquid phases, which deteriorates in quality below the triple point in the solid phase. This is highlighted by the post Mach shock temperature and purely dimensional differences between the Peng–Robinson predictions and those of the three-phase-accurate composite equation of state which predicts the

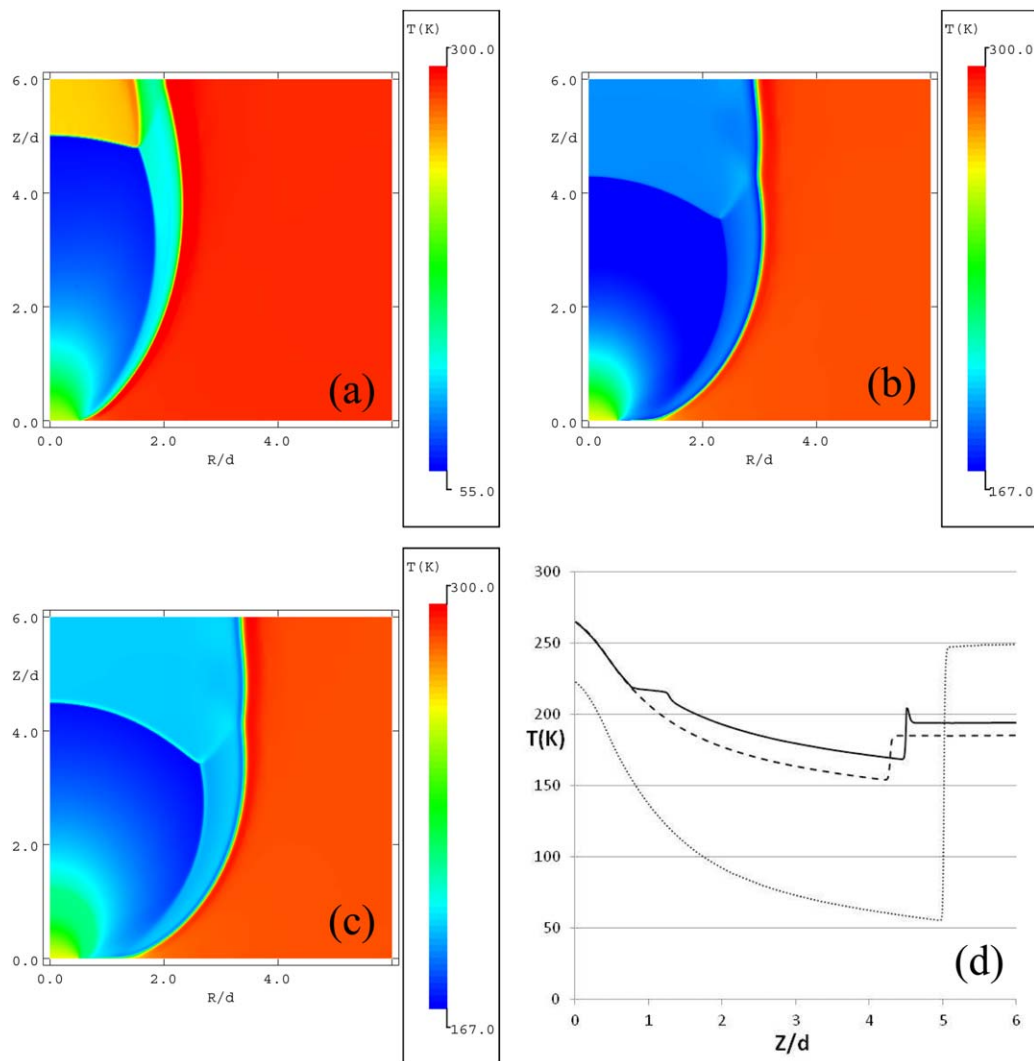


Figure 8. Temperature in the near-field of the flow domain.

This figure shows the temperature structure of the jet predicted by the ideal equation of state (a), the Peng–Robinson equation of state (b) and the composite equation of state (c). In panel (d), we show a comparison along the jet axis between the three models—ideal (dotted line), Peng–Robinson (dashed line), and composite (solid line). [Color figure can be viewed in the online issue, which is available at wileyonlinelibrary.com.]

correct post Mach shock temperature in this homogeneous equilibrium model. As expected, between the Peng–Robinson and composite approaches, the temperatures agree in the expansion until the triple point is reached, at which point the Peng–Robinson equation of state continues smoothly, whereas the composite equation of state model accounts for the latent heat of fusion change to the solid phase, and the temperature profiles diverge. The temperatures predicted here by all three equations of state are clearly low enough to make it absolutely crucial that an accurate three-phase equation of state for CO_2 is used to model these depressurizations.

Figure 9 shows the magnitude of velocity in the near-field of the jet resulting from the three different approaches. Note that the initial velocity of the ideal model is different because pressure and mass-flow have been conserved in the initial condition. The ideal equation of state predicts a high velocity in the expansion and annulus regions—between 400 and 600 m/s. In contrast, the Peng–Robinson and composite equations of state predict a velocity approaching 400 and 450 m/s, respectively, in the expansion fan just before the Mach shock. Further, the ideal equation of state does not predict any velocity

differences across the expansion fan, although a slow core and fast annulus become apparent postshock. Contrastingly, the Peng–Robinson and composite equations of state predict velocities around 200 m/s surrounding the expansion fan and into the annulus, encasing a similarly slow moving core. The annulus velocities are a factor of two less than for the ideal equation of state. Oblique shock waves originating from the shock triple point are also clear in the results from the Peng–Robinson and composite equations of state at the same levels. The lower right panel in Figure 9 shows the magnitude of velocity along the cylindrical axis of the jet. The Peng–Robinson and composite equations are again in agreement until the temperature reaches the triple point, at which the internal energy released during the formation of solid is converted to kinetic energy (the scheme is energy conserving) driving a secondary expansion of the jet and leading to a wider expansion fan, larger Mach shock and higher preshock velocities. Post Mach shock, the velocities from the Peng–Robinson and composite equations of state are in good agreement, whereas the ideal model predicts much larger velocities, again demonstrating the inapplicability of the ideal approach.

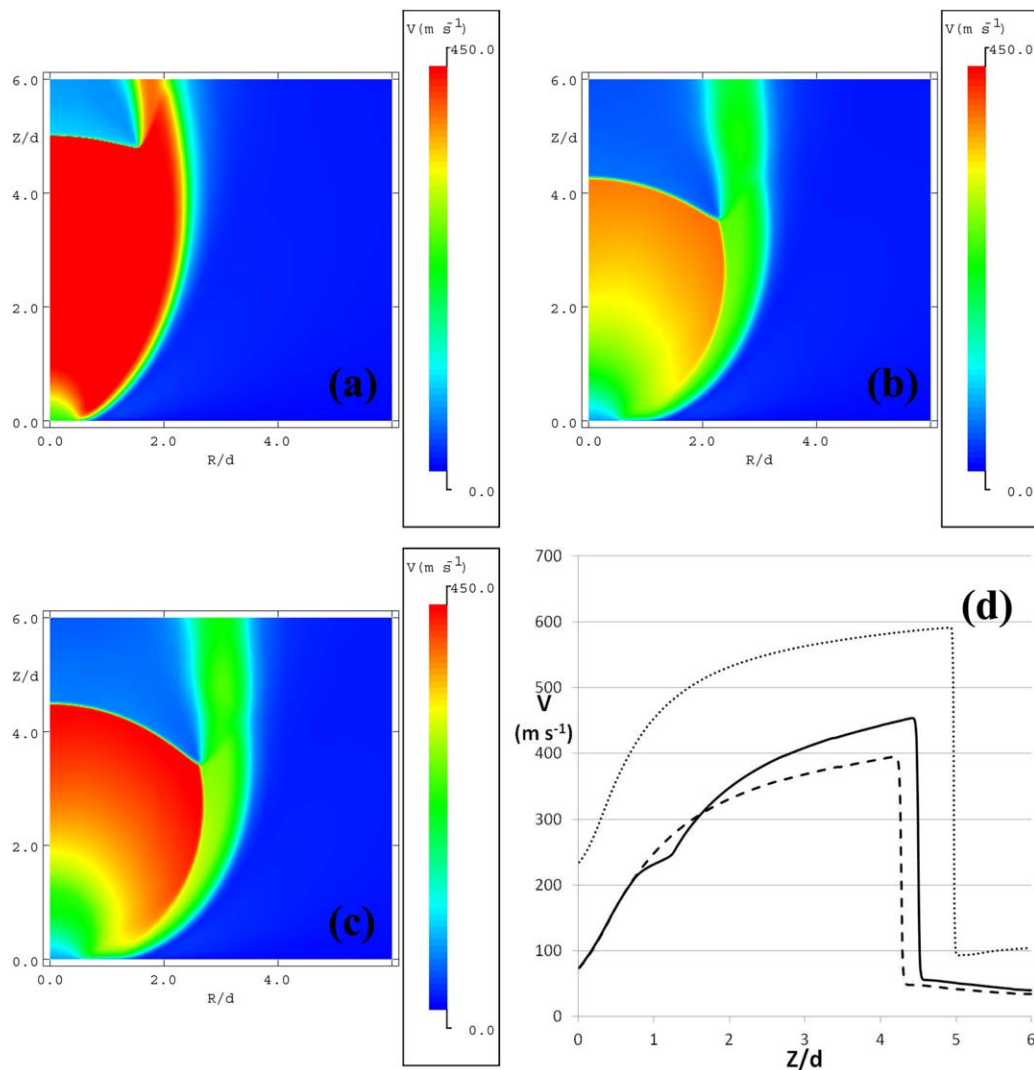


Figure 9. Magnitude of velocity in the near-field of the flow domain.

This figure shows the magnitude of velocity of the jet predicted by the ideal equation of state (a), the Peng–Robinson equation of state (b) and the composite equation of state (c). In panel (d), we show a comparison along the jet axis between the three models—ideal (dotted line), Peng–Robinson (dashed line) and composite (solid line). [Color figure can be viewed in the online issue, which is available at wileyonlinelibrary.com.]

Figure 10 shows the pressure in the flow domain. All three models have the same pressure at the nozzle, as defined by the conservation of pressure and mass-flow in the initial conditions. They begin to diverge immediately, although this is only clear in panel (d) of the figure after the pressure drops through the triple point pressure (0.518 MPa, 5.71 on the y axis of panel (d)). The composite and Peng–Robinson models remain similar, although the effect of correctly accounting for the latent heat of fusion is clear where the abrupt gradient change occurs at the triple point along the composite prediction (solid line panel (d)). Post Mach shock all three models return to atmospheric pressure as would be expected, although the position of the Mach shock is clearly incorrectly predicted by an ideal equation of state, once again demonstrating the lack of suitability of this ideal approach. The composite equation of state predicts that the Mach shock should be slightly further downstream than the Peng–Robinson equation of state.

Figure 11 gives the fraction of CO_2 in the domain. Pure CO_2 fills the entire expansion fan, the post Mach shock core and annulus in all three cases. Mixing is confined to a very

narrow region at the outer radial edge of the jet. This is likely to be the reality around the expansion fan, but beyond the Mach shock this is unlikely to be realistic—we discuss this further below. Note though that mixing region at the edge of the ideal jet is thinner than the mixing regions at the edges of the Peng–Robinson and composite jets.

Figure 12 shows the fraction of CO_2 in the condensed phase predicted by the Peng–Robinson and composite equations of state. No results are shown from the ideal equation of state as this is a gas-phase model with no condensed phase. Close to the release point, before the temperature drops below the triple point, the condensed CO_2 is in the liquid phase and the two approaches show identical predictions. Dramatic differences become apparent once the triple point temperature is reached and the liquid-phase CO_2 solidifies. The Peng–Robinson equation of state smoothly predicts a continuous fraction in the condensed phase as the temperature drops through the triple point—clearly unphysical as it implies a zero latent heat of fusion. In contrast, the composite equation of state, which correctly models the phase change from liquid to solid, shows a rapid decrease in the

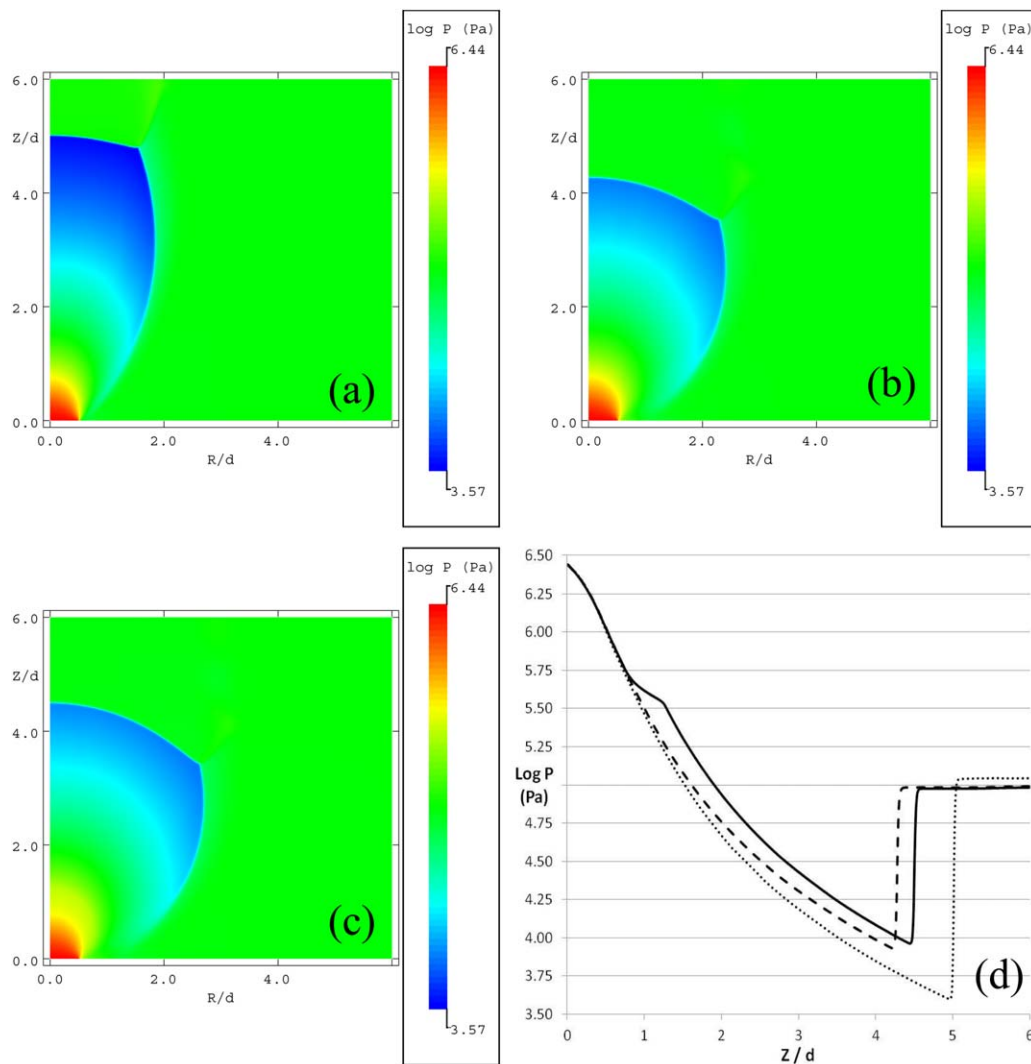


Figure 10. Pressure in the near-field of the flow domain.

This figure shows the pressure in the jet predicted by the ideal equation of state (a), the Peng–Robinson equation of state (b) and the composite equation of state (c). In panel (d), we show a comparison along the jet axis between the three models—ideal (dotted line), Peng–Robinson (dashed line), and composite (solid line). [Color figure can be viewed in the online issue, which is available at wileyonlinelibrary.com.]

amount of condensed-phase material as the temperature passes through the triple point, in agreement with the energy requirements of forming solid. Although the Peng–Robinson equation of state is strictly inapplicable beyond the point at which the material temperature drops below the triple point in the expansion fan, the predicted fractional change across the Mach shock is in agreement with the composite equation of state which is applicable in this regime. The fraction of solid CO_2 present after the Mach shock is considerably lower in the composite model than in the Peng–Robinson case, as expected when the latent heat of fusion is accounted for.

Discussion

Choice of the equation of state to use numerically is a balance between the accuracy of calculation and computational time. For example, certain computer codes utilize lookup tables of thermophysical properties rather than an explicit equation. This is usually done because calculating such properties in real time can be very computationally expensive. Hence, we have employed lookup tables for Span and

Wagner rather than the complete formulation which would be prohibitively expensive for the type of calculations reported here. We have seen the same level of performance between the Peng–Robinson and composite models, that is, we find no performance penalty in using the improved three-phase equation of state with tabulated data rather than a single explicit equation. We have also assumed that sound speed is independent of temperature and pressure. We have found that the results are extremely insensitive to the sound speed and also our choice for calculating solid density, as also employed by other authors.⁷

The results shown in the previous section have demonstrated the differences between using various equations of state in the calculation of sonic jets of CO_2 . Clearly, an ideal equation of state is unsuitable due to its lack of realism, and as it predicts incorrect dimensions of the near-field structure of such jets, as well as incorrect temperatures and velocities. Further, the method does not include the condensed phase which has been demonstrated to be fundamentally important for these releases. The Peng–Robinson equation of state, like many others used for CO_2 , is a two-phase equation of state

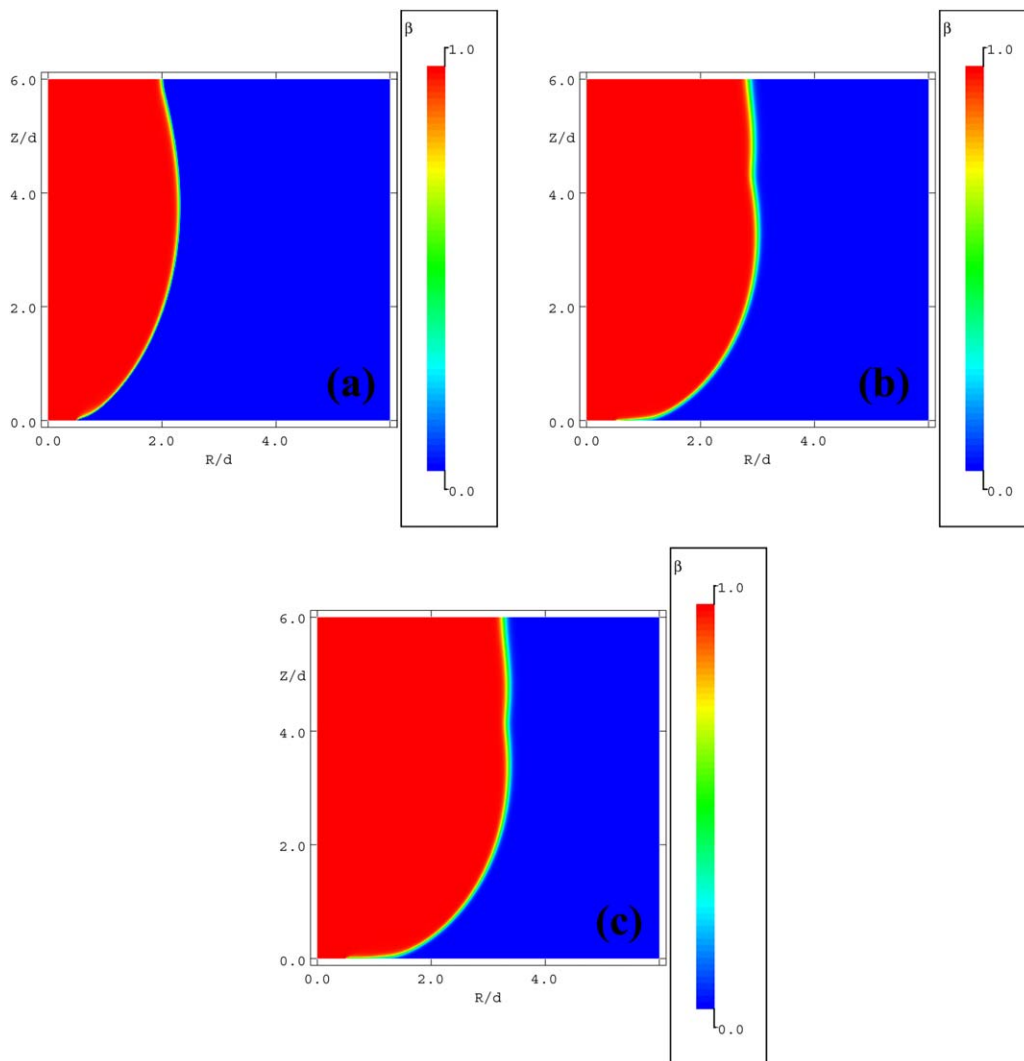


Figure 11. Concentration of CO₂ in the near-field of the flow domain.

This figure shows the amount of CO₂ in the jet predicted by the ideal equation of state (a), the Peng–Robinson equation of state (b) and the composite equation of state (c). [Color figure can be viewed in the online issue, which is available at wileyonlinelibrary.com.]

which is, in general, as accurate as any other for this situation above the triple point. However, the results in the previous section have highlighted the need for an equation of state which accurately handles the solid phase and the transition to it, hence we have developed the composite form detailed here.

During the development of this composite equation of state, we also examined the suitability of a number of other formulations. We considered the PRSV,²¹ PRSV-2,²² and GERG 2004⁶ (which is fundamentally based on the Span and Wagner method) equations. Whilst all these provided comparable results in the gas and liquid phases, none are applicable below the triple point. We have also considered the three-phase equation of state developed by Yokozeki²³; however, whilst the latent heat of fusion may be included, the method is difficult to implement computationally as continuous derivatives are required, the presence of which are not clear from Yokozeki's description. An improvement to this method may be gained by using Yokozeki's equation, with appropriate computational smoothing, but as we are already using the most accurate equation of state—Span and Wagner—we have not used Yokozeki's equation as it is complex

with a relatively large number of terms and parameters. So, for the purposes of examining the performance of our composite approach, we chose the Peng–Robinson equation of state given its simplicity to implement in a computational method. The composite method itself can be implemented with any of the equations of state noted above via lookup tables constructed from the chosen approach. The method will still correctly account for the latent heat of fusion and solid phase, as is required for simulations of high-pressure releases of CO₂ into air.

We have also repeated the entire set of simulations discussed using a fully turbulent RANS approach, closed using a compressibility corrected²⁴ $k-\epsilon$ turbulence model. These simulations are consistent with those presented here, revealing essentially the same behavior. As expected, the main effect of the inclusion of flow turbulence is to widen the mixing region at the edge of the jet in the near-field.

The results presented here consider flows similar to Yamamoto et al.²⁵ In their work, CO₂ flows through a nozzle with upstream pressures up to 2 MPa were considered. The upstream temperatures considered were above the critical temperature (400 and 600 K), although in the expansion

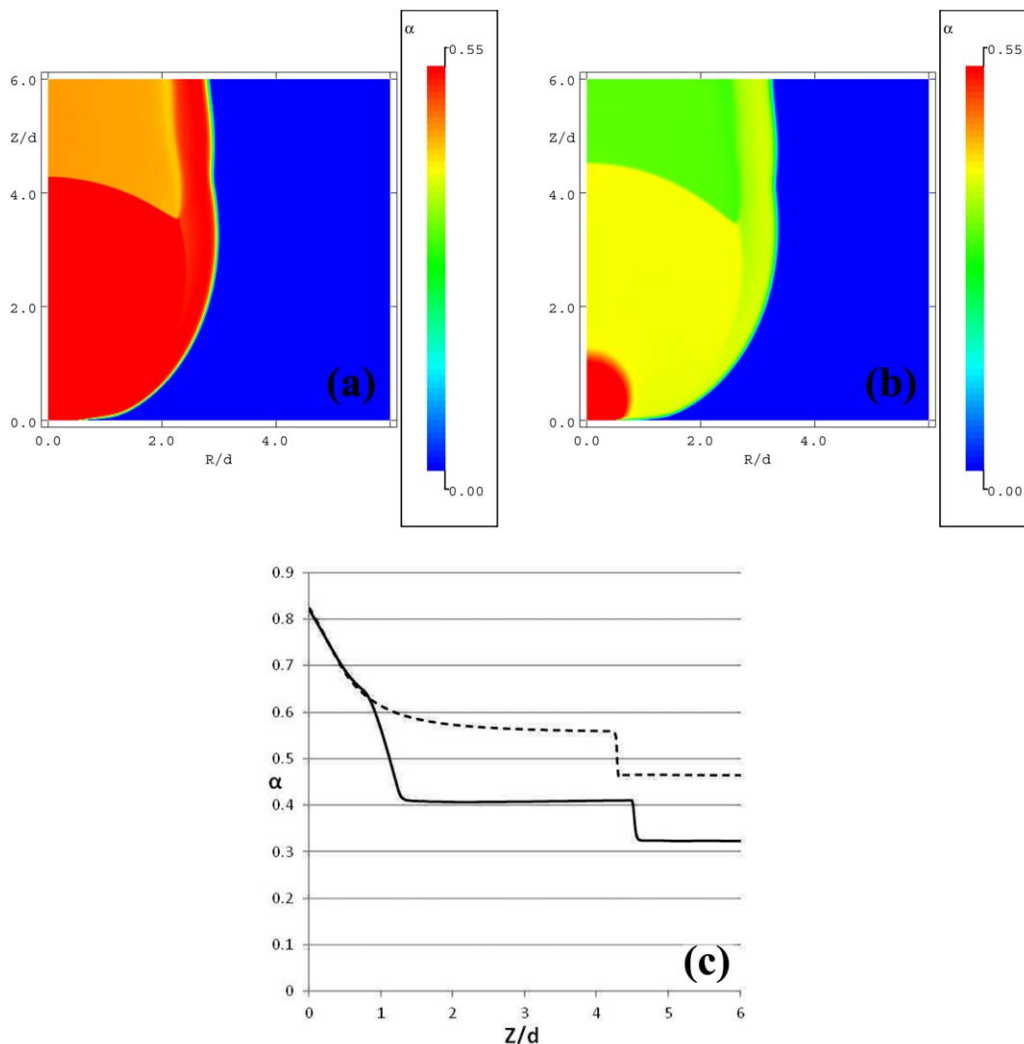


Figure 12. Concentration of condensed-phase CO₂ in the near-field of the flow domain.

This figure shows the amount of condensed-phase CO₂ as a fraction of the total CO₂ in the jet predicted by the Peng–Robinson equation of state (a) and the composite equation of state (b). In panel (c), we show a comparison along the jet axis between the two models—Peng–Robinson (dashed line) and composite (solid line). [Color figure can be viewed in the online issue, which is available at wileyonlinelibrary.com.]

temperatures dropped below the critical point. The authors employed the PROPATH thermophysical library for tabulating the thermophysical properties of CO₂. However, this library is only applicable above the triple point (the reference manual indicates most functions are applicable down to 220 K, but some only down to 240 K). Their results lend support to our results, but unlike Yamamoto et al. and the PROPATH library, our composite equation of state and fluid flow predictions are trans-triple-point and applicable to the CCS industry.

Conclusions

We have developed a new two-phase composite method of predicting the thermophysical properties of the three phases of CO₂ for the range of temperatures of relevance to CO₂ dispersion from releases at sonic velocities, of interest to the carbon capture and storage industry and in other applications. This new equation of state has been implemented in a way that is convenient for CFD applications; the gas phase is computed from the Peng–Robinson equation of state, and the liquid and condensed phases from tabulated data

generated with the Span and Wagner equation of state and the DIPPR® Project 801 database. Saturation pressure, gas- and condensed-phase densities, sound speed, and internal energy have all been tabulated against temperature, providing the basis for a fully functional form for differentiation, interpolation, and extrapolation in numerical simulations. No discontinuity or loss of accuracy at the critical point or anywhere along the saturation curve has been encountered by using this composite approach with different equations of state, as we have ensured that the Helmholtz free energy has continuous first derivatives.

A set of steady-state simulations has been performed to investigate the physical conditions in high-pressure releases of CO₂ into air and to compare predictions employing three different equations of state approaches: an ideal gas, the Peng–Robinson equation, and the new composite approach. The simulations have all shown that the material temperature of CO₂ drops below the triple point when released into air from high pressure. The new composite equation of state described in this article fully accounts for the triple-point limitation of other equations of state in modeling these releases by correctly including the solid-phase properties, for

example, density, and the transition to the solid phase, that is, the latent heat of fusion. Predictions from the composite approach show agreement with Peng–Robinson and Span and Wagner above the triple point, as expected, with physically realistic predictions below the triple point; unlike the other approaches, the composite method correctly predicts the pure CO₂ mixture of solid and gas to be at the experimentally measured sublimation temperature at atmospheric pressure. These simulations have demonstrated that it is absolutely crucial to employ a three-phase equation of state to model atmospheric dispersion of high-pressure CO₂.

Future developments of the composite approach will include the adoption of a suitable particle model and transport method. Without including these, further alterations of the equation of state employed in the gas phase or liquid phase will achieve no greater accuracy than the model presented here. An improved equation for the solid may be desirable, but will make almost no difference to the results presented here. Possibilities of extending this approach for the transport of CO₂ with impurities (e.g., a small fraction of nitrogen) exist by adjusting the liquid- and gas-phase behavior, but are beyond the scope of this article. Additionally, the publication of experimental data on the near-field structure of these releases would allow for a more complete validation of the composite equation of state approach.

Acknowledgments

CJW was supported under the COOLTRANS project funded by an industrial partnership grant from National Grid, and CJW and MF would like to thank National Grid for their support of the work described herein. National Grid has initiated the COOLTRANS programme of research to address knowledge gaps relating to the safe design and operation of onshore pipelines for transporting dense phase CO₂ from industrial emitters in the UK to storage sites offshore.

Notation

Roman letters

a = model parameter
 b = model parameter
 c = adiabatic sound speed
 C = specific heat
 d = nondimensional nozzle diameter
 e = total energy per unit volume
 F = Helmholtz free energy
 k = turbulence kinetic energy
 m = mass
 p = pressure
 r = nondimensional radial location
 R = universal gas constant
 t = time
 S = entropy
 T = temperature
 u = magnitude of velocity
 U = internal energy per unit mass
 v = molar volume
 w = molecular weight
 z = nondimensional axial location

Greek letters

α = condensed phase fraction
 β = total mass fraction of CO₂
 δ = Peng–Robinson equation of state parameter
 ϵ = dissipation rate of k
 γ = ratio of specific heats
 μ = molecular viscosity

ρ = density
 τ = relaxation time
 ω = acentric factor of the species

Subscripts

0 = reference state
 a = air
 c = condensed phase
 crit = critical point
 g = gas
 i = initial
 mix = mixture
 s = saturation
 trip = triple point
 v = vapor

Literature Cited

- Mazzoldi A, Hill T, Colls JJ. CO₂ transportation for carbon capture and storage: sublimation of carbon dioxide from a dry ice bank. *Int J Greenhouse Gas Control*. 2008;2:210–218.
- Connolly S, Cusco L. Hazards from high pressure carbon dioxide releases during carbon dioxide sequestration processes. In: IChemE Symposium Series No. 153, Edinburgh, UK, May 22–24, 2007, published by IChemE, Rugby, UK, 1–5.
- Wilday AJ, McGillivray A, Harper P, Wardman M. A comparison of hazard and risks for carbon dioxide and natural gas pipelines. In: IChemE Symposium Series No. 155, Manchester, UK, Nov. 10–12, 2009, published by IChemE, Rugby, UK, 392–398.
- Peng DY, Robinson DB. A new two-constant equation of state. *Ind Eng Chem Fundam*. 1976;15:59–64.
- Span R, Wagner W. A new equation of state for carbon dioxide covering the fluid region from the triple-point temperature to 1100 K at pressures up to 800 MPa. *J Phys Chem Ref Data*. 1996;25:1509–1596.
- Kunz O, Klimeck R, Wagner W, Jaeschke M. GERG Technical Monograph 15: The GERG-2004 wide-range equation of state for natural gases and other mixtures technical report. Ruhr-universitat Bochum, 2007.
- Witlox HWM, Harper M, Oke A. Modelling of discharge and atmospheric dispersion for carbon dioxide release. *J Loss Prev Proc Ind*. 2009;22:795–802.
- Liu L-G. Compression and phase behavior of solid CO₂ to half a megabar. *Earth Planet Sci Lett*. 1984;71:104–110.
- Hulsbosch-Dam C, Spruijt M, Necci A, Cozzani V. An approach to carbon dioxide particle distribution in accidental releases. *Chem Eng Trans*. 2012;26:543–548.
- Jacobson MZ. Fundamentals of Atmospheric Modelling. Cambridge University Press, Cambridge, UK, 1999.
- Falle SAEG. Self-similar jets. *Mon Not R Astron Soc*. 1991; 250:581–596.
- Godunov SK. A difference scheme for numerical computation of discontinuous solutions of equations of fluid dynamics. *Math Sbornik*. 1959;47:271–306.
- van Leer B. Towards the ultimate conservative difference scheme. IV. A new approach to numerical convection. *J Comput Phys*. 1977;23:276–299.
- Harten A, Lax PD, van Leer B. On upstream differencing and Godunov-type schemes for hyperbolic conservation laws. *SIAM Rev*. 1983;25:35–61.
- Falle SAEG. AMR applied to non-linear Elastodynamics. In: Plewa T, Linde T, Weirs VG, editors. The Proceedings of the Chicago Workshop on Adaptive Mesh Refinement Methods. *Springer Lecture Notes in Computational Science and Engineering*, vol. 41. New York: Springer, 2005:235–253.
- Essandoh-Yeddu J, Gülen G. Economic modeling of carbon dioxide integrated pipeline network for enhanced oil recovery and geologic sequestration in the Texas Gulf Coast region. *Energy Procedia*. 2009;1:1603–1610.
- Mahgerefteh H, Oke A, Atti O. Modelling outflow following rupture in pipeline networks. *Chem Eng Sci*. 2006;61:1811–1818.
- Mahgerefteh H, Saha P, Economou IG. Fast numerical simulation for full bore rupture of pressurized pipelines. *AIChE J*. 1999;45:1191–1201.
- Mahgerefteh H, Denton G, Rykov Y. A hybrid multiphase flow model *AIChE J*. 2008;54:2261–2268.
- Barber CR. The sublimation temperature of carbon dioxide. *Br J Appl Phys*. 1966;17:391–397.

21. Stryjek R, Vera JH. PRSV: an improved Peng–Robinson equation of state for pure compounds and mixtures. *Can J Chem Eng.* 1986;64:323–333.
22. Stryjek R, Vera JH. PRSV2: a cubic equation of state for accurate vapor–liquid equilibria calculations. *Can J Chem Eng.* 1986;64:820–826.
23. Yokozeki A. Solid–liquid–vapor phases of water and water–carbon dioxide mixtures using a simple analytical equation of state. *Fluid Phase Equilib.* 2004;222:55–66.
24. Sarkar S, Erlebacher G, Hussaini MY, Kreiss HO. The analysis and modelling of dilatational terms in compressible turbulence. *J Fluid Mech.* 1991;227:473–493.
25. Yamamoto S, Matsuzawa R, Furusawa T. Simulation of thermophysical flow in axisymmetric nozzle with expansion chamber. *AIChE J.* 2011;57:2629–2635.

Manuscript received July 20, 2012, and revision received Mar. 12, 2013.
